Epitaxial growth, perpendicular magnetic anisotropy, and domain structure of Co/Pt(311) and (111) multilayers

J. C. A. Huang, L. C. Wu, A. C. Hsu, and Y. M. Hu
Physics Department, National Cheng-Kung University, Tainan, Taiwan

T. H. Wu
Department of Humanities and Science, National Yunlin University of Science and Technology, Touliu, Taiwan

C. H. Lee
Department of Engineering and System Science, National Tsing-Hua University, Hsinchu, Taiwan
(Received 22 June 1998; revised manuscript received 25 August 1998)

We have simultaneously grown $[\mathrm{Co}(t\ \text{Å})/\mathrm{Pt}(10\ \text{Å})]_{30}$ ($t=2-10$ Å) multilayers on Pt(311) and Pt(111) planes by molecular beam epitaxy. The Pt(311) and Pt(111) seeding layers were prepared on $\mathrm{Mo}(211)/\mathrm{Al_2O_3}(1\bar{1}00)$ and $\mathrm{Mo}(110)/\mathrm{Al_2O_3}(11\bar{2}0)$, respectively. New epitaxial relations between Pt and Mo layers in both cases are established by electron and x-ray diffraction. The Co/Pt multilayers on Pt(311) were grown mainly as a (311) structure but mixed with a small amount of (211) phase. The Co/Pt(311) multilayers display large perpendicular magnetic anisotropy with results comparable to those of the (111) samples. In addition, the Co/Pt($3\bar{1}1$) multilayers exhibit stripelike magnetic domain structure with domain displacement growing along the $[0\bar{1}1]$ azimuth, in marked contrast to the (111) multilayers which show a very irregular domain structure. [S0163-1829(99)04401-X]

The magnetism of magnetic multilayers (ML's) composed of modulated ferromagnetic-nonferromagnetic (F-NF) layers and magnetic thin films have attracted much attention in recent years. For instance, Co/Pt multilayers[1–7] and ordered alloy films[8–11] with large perpendicular magnetic anisotropy (PMA) and Kerr rotations have received considerable interest both for basic research and application for high-density storage. Reduced dimensionality of the magnetic layers (to a few monolayers) together with the symmetry breaking in the F-NF interfaces of the ML's, or in ordered alloys for similar reasons, can result in the change of magnetic property from in-plane to perpendicular alignment.[1–11] In addition, the interfacial strain and polarization effect in the F-NF interfaces are also important to the PMA effect. The *interfacial* structure, such as the interfacial roughness or alloy formation, thus plays an important role in determining the PMA effect.[1,8–11]

It has also been demonstrated that PMA and other magnetic properties depend sensitively on the crystal *orientation* in the Co/Pt ML's.[2,6,7] For instance, the (111)-oriented Co/Pt ML's exhibit much enhanced PMA effects compared to the other low-index planes such as the (100) and (110) growth orientations. Most of the previous studies had been focused on low-indexed-orientation films which exhibit a large PMA effect. Much less work was devoted to study films or ML's with high-indexed orientations. The difficulty lies in the sample preparation in the first place. Indeed, the thermal stability and ordering of the high-indexed planes such as the $(n11)$ surfaces are of fundamental interest and importance.[12,13] In this investigation, we study the epitaxial growth, crystal and interfacial structure, as well as the PMA effect in mainly (311)-oriented Co/Pt ML's grown on Pt/Mo seeding layers. For comparison, we also study Co/Pt(111) ML's simultaneously prepared with the (311) samples. Epitaxial relations between Pt and Mo seeding layers in both cases are reported. The interplay between the crystal orientation and magnetic domain structure in these systems are also discussed.

The crystal growth of the Co/Pt ML's was carried out by a Vacuum Product made molecular beam epitaxy system (MBE-930). Details of the chamber in which the crystal growth took place are provided elsewhere.[14,15] To enable the growth of high-quality samples, the sapphire substrates were chemically precleaned and then introduced into the growth chamber and outgased at about 1000 °C for 1 h under ultrahigh-vacuum conditions before initial deposition. Pure (99.99%) Mo, Pt, and Co elements were evaporated from a separate *e*-beam source. The (311) and (111) $[\mathrm{Co}(t\ \text{Å})/\mathrm{Pt}(10\ \text{Å})]\times 30$ ($t=2$, 2.5, 3, 4, 5, and 10 Å) ML's were grown on 200 Å Pt/200 Å Mo seeding layers onto epitaxial grade $\mathrm{Al_2O_3}(1\bar{1}00)$ and $\mathrm{Al_2O_3}(11\bar{2}0)$ substrates, respectively. The epitaxy of the Co/Pt(111), (110), and (100) ML's had been firmly established by employing GaAs substrates and using Ag and Pt as the seeding layers.[1,2]

The base pressure of the MBE system is of about 2×10^{-10} Torr. During deposition of the Co/Pt ML's, the growth pressure was controlled below 5×10^{-9} Torr, the deposition rates at ~0.05–0.1 Å/sec. To retain the sample uniformity the sample holder was rotated with a constant speed of about 30 rpm. The substrate temperatures were kept at optimal[16] conditions ($\sim T_m/3$) of 900 °C for the Mo seeding layer and 500 °C for the Pt seeding layer. The Co/Pt ML's were grown at room temperature to avoid interdiffusion between the Co and Pt layers.

The surface and bulk crystal structures of the Co/Pt ML's were investigated by reflection-high-energy-electron diffraction (RHEED) and x-ray diffraction (XRD), respectively. Magnetic hysterisis loops and the magnetization values were

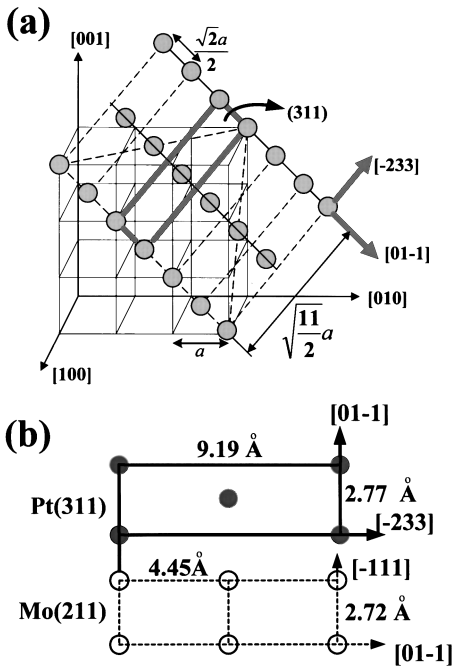

FIG. 1. Schematic diagrams showing (a) the lattice geometry and unit cell (indicated by bold lines) of the fcc (311) plane and (b) epitaxial relations of the Pt(311) and Mo(211).

measured by polar magneto-optical Kerr effect (PMOKE) and vibrational sample magnetometer (VSM), respectively. The PMOKE and VSM measurements were carried out at room temperature in a magnetic field H up to 20 kOe. Note that the penetration depth[17] of the He-Ne laser ($\lambda = 632.8$ nm) is of about 200 Å, so only about the top 10–15 (Co/Pt) bilayers can be probed by PMOKE. Magnetic domain structures of the Co/Pt ML's were observed by employing a polar Kerr microscope and a magnetic force microscope (MFM) equipped with a phase detection module. The magnetic tip with a CoCr-coated Si tip magnetized along the tip axis was used to scan the magnetic domain structures in the MFM tapping-lift mode. Domain images represent the detected frequency shift of the vibrating cantilever. It has been shown[18] that MFM contrast can be associated with up- and down-magnetized domains.

For Co/Pt ML's studied here we have decided (by RHEED and XRD) the following orientation

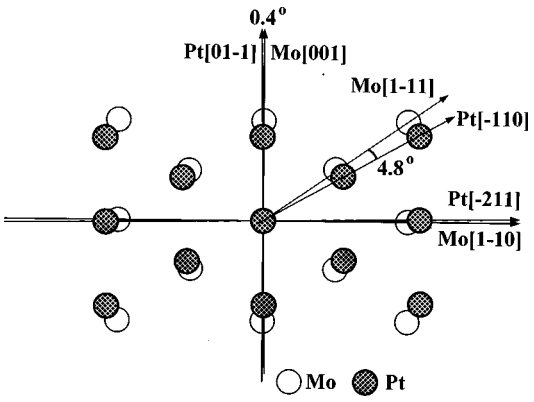

FIG. 2. Schematic diagram showing the in-plane epitaxial relations of the Pt(111) and Mo(110).

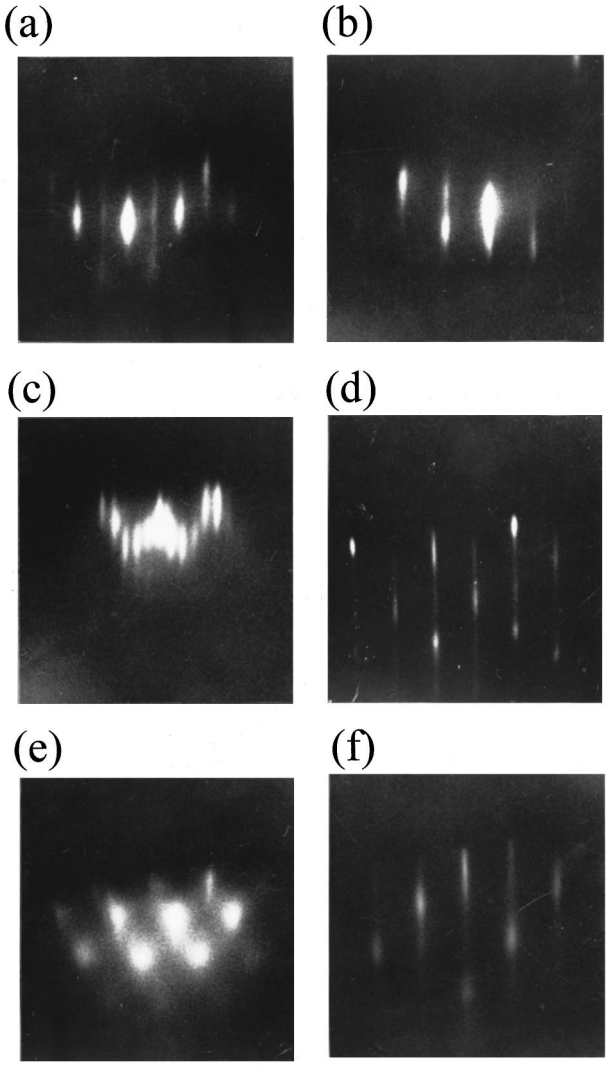

FIG. 3. RHEED patterns for (a), (b) 200 Å Mo(211), (c), (d) 200 Å Pt(311), and (e), (f) the subsequent (top Co layers of) $[Co(3\,Å)/Pt(10\,Å)]_{30}$ multilayers. The RHEED beam was directed along the Mo[011] for (a), (c), and (e), and along the Mo[111] for (b), (d), and (f).

relations (OR's) for the (311) ML's: fcc ML's $(\underline{3}11)\|fcc\ Pt(311)\|bcc\ Mo(211)\|Al_2O_3(1\underline{1}00)$, ML's $[0\underline{1}1]\|Pt[0\underline{1}1]\|Mo[1\underline{1}1]\|Al_2O_3[000\underline{1}]$, and ML's $[\underline{2}33]\|Pt[\underline{2}33]\|Mo[0\underline{1}1]\|Al_2O_3[11\underline{2}0]$. Detailed tilt XRD scans[19] show that the (311) ML's are mixed with a small amount of twinned (211) phase[17] possibly for large lattice mismatch (about 10%) between the Co and Pt lattice spacings. Schematic diagrams of the lattice geometry and the epitaxial relations between the fcc Pt(311) and bcc Mo(211) planes are provided in Fig. 1. Note that the growth of Pt(311) on the Mo(211) plane is due to the good match of both the 2D cells and the atomic densities. The unit cell of Pt(311) plane, 2.77 Å×9.19 Å, fits very well with two repeat cells of the Mo(211), 2.72 Å×4.45 Å, as illustrated in Fig. 1. In addition, the atomic density for the Pt(311) plane, 0.079 $Å^{-2}$, is rather close to that of the Mo(211) plane, 0.082 $Å^{-2}$.

For Co/Pt(111) ML's the out-of-plane OR was determined as fcc ML's$(111)\|fcc\ Pt(111)\|bcc\ Mo(110)\|Al_2O_3(11\underline{2}0)$. Tilt XRD scans indicate that the in-

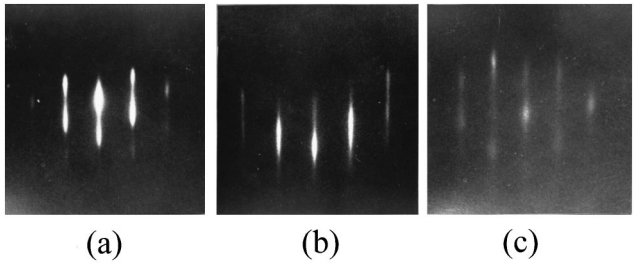

FIG. 4. RHEED patterns for (a) 200 Å Mo(110), (b) 200 Å Pt(111), and (c) the subsequent (top Co layers of) $[Co(3\ Å)/Pt(\underline{1}0\ Å)]_{30}$ multilayers. The RHEED beam was directed along the Mo[110] for (a), and along the fcc [211] for (b) and (c).

plane OR for Pt(111) on Mo(110) layers is neither the Kurdjumov-Sachs (KS, fcc[111]‖bcc[$\underline{1}11$]) nor exactly the Nishiyama-Wassermann (NW, fcc[110]‖bcc[001]) relationship.[20,21] Instead, it is closer to the NW orientation but with the fcc Pt[$\bar{1}10$] azimuth rotated with a unique sense[22] by ~0.4° from the bcc Mo[001], as determined by the in-plane x-ray diffraction. The in-plane epitaxial relations between Pt(111) and Mo(110) are schematically illustrated in Fig. 2.

Typical RHEED patterns of the Mo(211) and subsequent Pt(311) layers are shown in Figs. 3(a) and 3(b) and 3(c) and 3(d), respectively. The subsequent growth of Co/Pt ML's remains mainly as (311) structure with however increased surface roughness [Figs. 3(e) and 3(f)] compared to the Pt(311) surface [Figs. 3(c)–3(d)]. Furthermore, RHEED observations [Figs. 4(a)–4(c)] show that the Co/Pt(111) ML's possess much smoother interfaces than those of the (311) ML's. The distinct interfacial roughness is also revealed by the XRD spectra where the (311) ML's show no satellite peaks [Fig. 5(a)] but the (111) ML's display clear superlattice satellites. [Fig. 5(b)]. The larger interfacial roughness of the Co/Pt(311) [compared to the (111) ML's] could be related to the factor of surface energy and strains between the Co and Pt layers. The effect of lattice strain is evidenced by the relatively large shift of the fundamental peak [indexed as Co/Pt(311) in Fig. 5(a)] in the (311) ML. This together with detailed radial XRD scans[22] (not shown here) reveal that there is as much as 2.8% contraction of the perpendicular lattice parameter in the Pt(10 Å) layers of the (311) ML's.

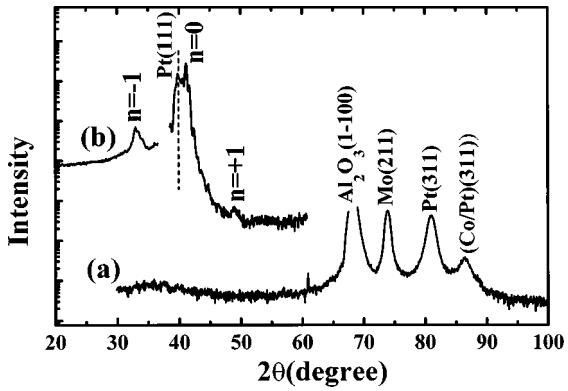

FIG. 5. X-ray diffraction spectra of $[Co(3\ Å)/Pt(\underline{1}0\ Å)]_{30}$ multilayers grown on (a) Pt(311)/Mo(211)/$Al_2O_3(1\bar{1}00)$ and (b) Pt(111)/Mo(110)/$Al_2O_3(11\bar{2}0)$.

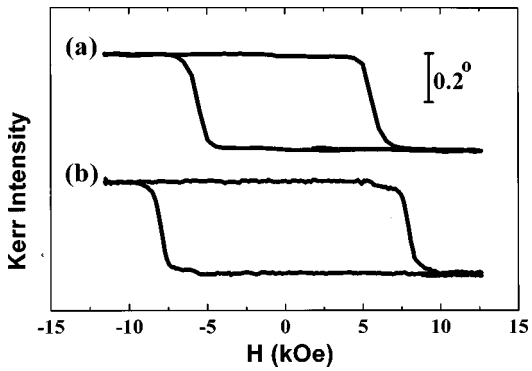

FIG. 6. PMOKE hysteresis loops of $[Co(3\ Å)/Pt(\underline{1}0\ Å)]_{30}$ multilayers grown on (a) Pt(311)/Mo(211)/$Al_2O_3(1\bar{1}00)$ and (b) Pt(111)/Mo(110)/$Al_2O_3(11\bar{2}0)$.

Details of the interfacial structure (such as the alloy formation) in the Co/Pt(311) or (111) ML's will be simulated by the fitting of XRD data for the future work.

By PMOKE we have studied the dependence of PMA

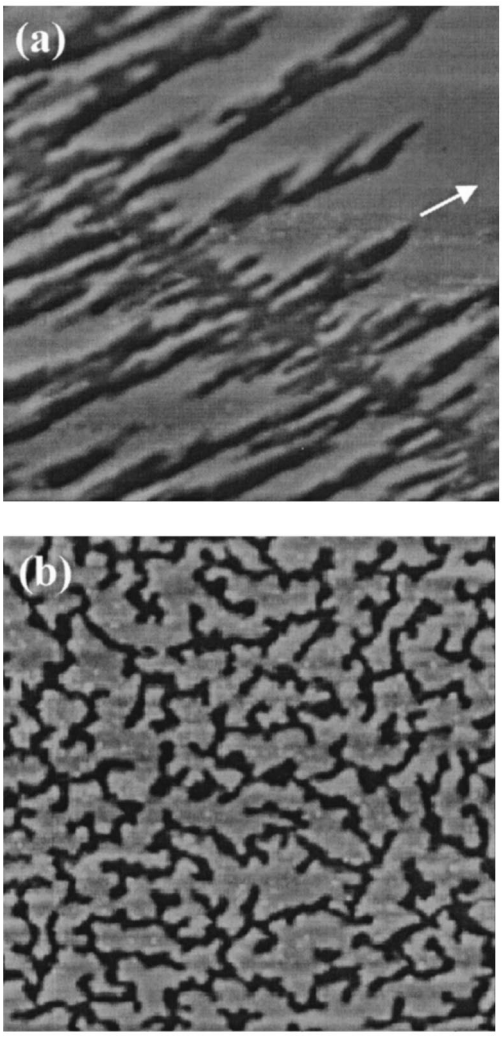

FIG. 7. MFM images scanned from $[Co(3\ Å)/Pt(\underline{1}0\ Å)]_{30}$ multilayers grown on (a) Pt(311)/Mo(211)/$Al_2O_3(1\bar{1}00)$ and (b) Pt(111)/Mo(110)/$Al_2O_3(11\bar{2}0)$. The arrow direction in (a) is parallel to the underlying Pt[011] azimuth. The scan areas are 15 μm×15 μm in both figures.

upon the Co thickness ($t_{Co}=2$, 2.5, 3, 4, 5, and 10 Å) for a fixed Pt thickness at 10 Å. The best PMA effects occur at $t_{Co}\sim 3$ Å for both the (311) and (111) ML's. The Co/Pt(311) ML ($t_{Co}=3$ Å) display large perpendicular magnetic anisotropy with loop squareness Sq=0.96, polar coercivity $H_c=5.6$ kOe, and Kerr rotation $\theta_k=0.2°$. The results of the (311) ML [Fig. 6(a)] are comparable to those (Sq=0.98, $H_c=7.8$ kOe, and $\theta_k=0.18°$) of the (111) ML [Fig. 6(b)], in marked contrast to the (110) and (100) oriented ML's which show a very poor PMA effect.[1,2]

From the M-H spectra measured by VSM (not shown here), the effective perpendicular magnetic anisotropic constant ($K_{eff}=K_v+2K_s/t_{Co}$) for the Co/Pt(111) and (311) ML's are obtained.[22] By linear fitting of the $t_{Co}K_{eff}$ versus t_{Co} curves, we have calculated the bulk anisotropic constant (K_v) as $\sim-(2-3)\times10^{-7}$ erg/cm^3 and the surface (or interface) anisotropic constant (K_s) as $\sim 0.1-0.15$ erg/cm^2 for our epitaxial Co/Pt ML's. The K_{eff} values in this work are slightly smaller than those reported[7,23] earlier by the other research groups.

For the domain structure studies, the Co/Pt ML's were demagnetized prior to the MFM measurements. During the demagnetization processes, the films were saturated in one direction by applying a perpendicular magnetic field greater than the coercivity H_c. Then, a magnetic field with opposite direction near the nucleation coercivity H_n was applied and the magnitude of the field was kept constant. Indeed a polar Kerr microscope was employed to monitor the developing of magnetic domains in a large area during the demagnetization process. After the magnetic domains had been developed, the magnetic field was turned off, and the sample was moved to the MFM stage for further observation. The growth of magnetic domains in both cases all show wall motion dominated (WMD) behavior. In the WMD case, domains nucleate from widely separated nucleation centers with low anisotropy defects. As observed from the polar Kerr microscope, the magnetization reversal processes started from the nucleation centers, then grew up via domain wall displacement. In addition, we find that the locations of the nucleation sites depend on the magnetic history of the samples.

Typical MFM images of the (311) and (111) ML's are displayed in Figs. 7(a) and 7(b), respectively. Interestingly, the (311) ML's exhibit stripelike magnetic domain structure and the domains grow quite uniformly along the in-plane fcc [011] azimuth as shown in Fig. 7(a). The reason is believed related to the crystal anisotropy of the fcc (311) surface and large strain between the Pt and Co elements in the ML's. The crystal anisotropy together with the lattice mismatch between the Co and Pt in turn could result in highly anisotropic defects along one ([011]) of the two ([011] and [233]) principle azimuths. Further measurements such as the cross-sectional TEM will be carried out for this investigation. On the other hand, the (111) ML's show much irregular (mazelike) and homogeneous domain structure as shown in Fig. 7(b), in marked contrast to those of the (311) ML's. The MFM results of the (111) ML's are likely related to the sixfold symmetry of the (111) plane.

In summary, we have prepared Co/Pt(311) and (111) ML's on Pt(311) and Pt(111) planes by molecular beam epitaxy. The high-indexed (311) plane of Pt is stabilized by the Mo(211) due to the excellent match of the atomic density and 2:1 ratio of the 2D unit cells. A new epitaxial relation between Pt(111) and Mo(110) interface is also established. The Co-Pt interfaces of the (311) ML's are much rougher than those of the (111) ML's due to the factor of surface energy. The (311) ML's display large PMA with results comparable to those of the (111) samples. Further, the (311) ML's exhibit stripelike magnetic domain structure and the domains grow quite regularly along specific crystalline azimuth, in marked contrast to the (111) ML's which show much uniform and irregular domain structure. We demonstrate that there is a strong correlation between the crystal orientation and the domain structure.

We are grateful for the financial support by the ROC NSC under Grant Nos. 87-2112-M-006-014 and 87-2732-M-006-001.

[1] R. F. C. Farrow, R. F. Marks, D. Weller, G. R. Harp, T. A. Rabedeau, M. F. Toney, and S. S. P. Parkin, Mater. Sci. Eng., R. **11**, 155 (1993).

[2] C. H. Lee, R. F. C. Farrow, C. J. Lin, E. E. Marinero, and C. J. Chien, Phys. Rev. B **42**, 11 384 (1990).

[3] R. F. Carcia, J. Appl. Phys. **63**, 5066 (1988).

[4] W. B. Zeper, F. J. A. M. Greidanus, P. F. Carcia, and C. R. Fincher, J. Appl. Phys. **65**, 4971 (1989); W. B. Zeper, H. W. van Kesteren, B. A. Jacobs, and J. H. M. Spruit, *ibid.* **70**, 2264 (1991).

[5] K. Babcock, V. B. Elings, J. Shi, D. D. Awschalom, and M. Dugas, Appl. Phys. Lett. **69**, 705 (1996).

[6] C. J. Lin and G. L. Gorman, Appl. Phys. Lett. **61**, 1600 (1992).

[7] C. L. Canedy, X. W. Li, and Gang Xiao, J. Appl. Phys. **81**, 5367 (1997).

[8] E. E. Marinero, R. F. C. Farrow, C. H. Lee, H. Notary, X. Yan, and T. A. Egami, Appl. Phys. Commun. **93**, 194 (1993).

[9] R. F. C. Farrow, D. Weller, M. F. Toney, T. A. Rabedeau, J. E. Hurst, G. R. Harp, R. F. Marks, R. H. Geiss, and H. Notary, in *Polycrystalline Thin Films: Structure, Texture, Properties and Applications*, edited by K. Barmak *et al.*, MRS Symposia Proceedings No. 343 (Materials Research Society, Pittsburgh, 1993), p. 375; E. E. Marinero, R. F. C. Farrow, G. R. Harp, R. H. Geiss, A. Bain, and B. Clemens, in *Magnetic Ultrathin Films: Multilayers and Surface/Interfaces and Characterization*, edited by B. T. Jonker *et al.*, MRS Symposia Proceedings No. 313 (Materials Research Society, Pittsburgh, 1993), p. 677.

[10] G. R. Harp, D. Weller, T. A. Rabedeau, R. F. C. Farrow, and M. F. Toney, Phys. Rev. Lett. **71**, 2493 (1993).

[11] R. W. Rooney, A. L. Shapiro, M. Q. Tran, and F. Hellman, Phys. Rev. Lett. **75**, 1843 (1995).

[12] K. Liang, E. B. Sirota, K. L. D'Amico, G. J. Hughes, and S. K. Sinha, Phys. Rev. Lett. **59**, 2447 (1987).

[13] A. Aslanides, M. Hayoun, and V. Pontikis, Surf. Sci. **370**, L163 (1997).

[14] J. C. A. Huang, T. E. Wang, C. C. Yu, Y. M. Hu, P. B. Lee, and

M. S. Yang, J. Cryst. Growth **171**, 442 (1997).
[15] J. C. A. Huang, Y. Liou, Y. D. Yao, W. T. Yang, C. P. Chang, S. Y. Liao, and Y. M. Hu, Phys. Rev. B **52**, R13 110 (1995).
[16] C. P. Flynn, J. Phys. F **18**, L195 (1988).
[17] J. C. A. Huang, Y. M. Hu, C. C. Yu, and C. H. Tsao, Phys. Rev. B **57**, 11 517 (1998).
[18] P. F. Carcia, A. D. Meinhaldt, and A. Suna, Appl. Phys. Lett. **47**, 178 (1985).
[19] C. H. Lee, J. C. A. Huang, and L. C. Wu (unpublished). The schematic diagram of the twinned fcc (211) structure can be found in Ref. 17.
[20] See, e.g., A. Zangwill, *Physics at Surfaces* (Cambridge University Press, Cambridge, 1988), p. 422.
[21] E. Bauer, Z. Kristallogr. **110**, 372 (1958).
[22] L. C. Wu, M. S. thesis, National Cheng-Kung University, Taiwan, 1998.
[23] J. Lin and G. L. Gorman, J. Magn. Magn. Mater. **93**, 194 (1993).